Journal of Neuroscience Research

Journal of Neuroscience Research 88:1695–1707 (2010)

Oligodendrogenesis in Iron-Deficient Rats: Effect of Apotransferrin

M.V. Rosato-Siri,[1] M.E. Badaracco,[2] E.H. Ortiz,[2] N. Belforte,[3] M. Guardia Clausi,[2] E.F. Soto,[2] R. Bernabeu,[1] and J.M. Pasquini[2]*

[1]Instituto de Biología Celular y Neurociencias ''Professor Eduardo De Robertis,'' Facultad de Medicina, Universidad de Buenos Aires, Buenos Aires, Argentina
[2]Departamento de Química Biológica, Facultad de Farmacia and Bioquímica and IQUIFIB-IIMHNO, Universidad de Buenos Aires-CONICET, Buenos Aires, Argentina
[3]Laboratorio de Neuroquímica Retiniana y Oftalmología Experimental, Departamento de Bioquímica Humana, Facultad de Medicina, Universidad de Buenos Aires and CEFyBO-Universidad de Buenos Aires-CONICET, Buenos Aires, Argentina

In rats, iron deficiency produces an alteration in myelin formation. However, there is limited information on the effects of this condition on oligodendroglial cell (OLGc) proliferation and maturation. In the present study, we further analyzed the hypomyelination associated with iron deficiency by studying the dynamics of oligodendrogenesis. Rats were fed control (40 mg Fe/kg) or iron-deficient (4 mg Fe/kg) diets from gestation day 5 until postnatal day 3 (P3) or 11 (P11). OLGc proliferation, migration and differentiation were investigated before and after an intracranial injection of apotransferrin at 3 days of age (P3). The proliferating cell population was evaluated at P3. Iron-deficient (ID) animals showed an increase in the oligodendrocyte precursors cell (OPC) population in comparison with controls. The overall pattern of migration of cells labeled with BrdU was investigated at P11. Iron deficiency increased the amount of $BrdU^+$ cells in the corpus callosum (CC) and decreased OLGc maturation and myelin formation. Changes in nerve conduction were analyzed by measuring visual evoked potentials. Latency and amplitude were significantly disturbed in ID rats compared with controls. Both parameters were substantially normalized when animals were treated with a single intracranial injection of 350 ng apotransferrin (aTf). The current results give support to the idea that iron deficiency increases the number of proliferating and undifferentiated cells in the CC compared with the control. Treatment with aTf almost completely reverted the effects of iron deficiency, both changing the migration pattern and increasing the number of mature cells in the CC and myelin formation.

Key words: myelin repair; iron deficiency; oligodendrocytes maturation; transferrin

Iron deficiency is one of the most common nutritional problems in the world. It has been reported that, in children under 2 years of age, the prevalence of iron deficiency is about 25% (Bamberg, 2008) and that such deficiency in infants is associated with a number of neural defects and hypomyelination (Dobbing, 1990). Work by different laboratories indicates that iron is an essential factor for normal myelination (Connor and Menzies, 1996; Ortiz et al., 2004) and that an increase in iron uptake is necessary for normal brain gliogenesis (Connor and Menzies, 1996).

Changes in iron availability affect oligodendroglial cell (OLGc) development during early embryogenesis (Morath and Mayer-Pröschel, 2001), and it has been hypothesized that the lack of myelin formation in iron-deficient (ID) animals is due mainly to a defect in myelin generation at early postnatal ages, when OLGcs complete their maturation. Myelin composition is strongly affected in ID animals (Beard et al., 2003; Ortiz et al., 2004; Badaracco et al., 2008).

The development of the central nervous system (CNS) is a process in which a pool of progenitor neural stem cells (NSCs) changes to a more specific phenotype. NSCs are identified by the expression of the polysialylated form of the cell surface glycoprotein NCAM (PSA-NCAM) and nestin. During maturation of OLGcs, the decrease of these two markers is accompanied by an increase in the expression of early markers of the OLGc lineage, such as A2B5 and O4 (Franco et al., 2008).

Oligodendrocyte precursor cells (OPCs) can be identified in vivo by the expression of the cell surface

The first two authors contributed equally to this work.

Contract grant sponsor: University of Buenos Aires B114; Contract grant sponsor: Agencia Nac. de Prom. de Ciencia y Tecnologia; Contract grant number: BID 1728 OC AR PICT 38201.

*Correspondence to: Juana M. Pasquini, PhD, Departamento de Química Biológica, Facultad de Farmacia and Bioquímica and IQUIFIB-IIMHNO, Universidad de Buenos Aires-CONICET, Junin 956, Buenos Aires, Argentina. E-mail: jpasquin@qb.ffyb.uba.ar

Received 28 July 2009; Revised 21 October 2009; Accepted 21 November 2009

Published online 1 February 2010 in Wiley InterScience (www.interscience.wiley.com). DOI: 10.1002/jnr.22348

marker NG2 (Levine and Nishiyama, 1996). Cells expressing NG2 are also abundant in different regions of the adult brain, which according to Greenwood and Butt (2003) could represent a new type of immature cell, different from neurons, OLGcs, and astrocytes. Morath and Mayer-Pröschel (2001) showed that iron impacts developmental processes acting on the proliferation of OPC. More recently, iron deficiency during pregnancy was found not only to affect the proliferation of glial cells but also to disturb, in an heterogeneous fashion, the generation of OLGcs from precursor cells (Morath and Mayer-Pröschel, 2002).

We have previously demonstrated that intracranially injected (ICI) apotransferrin (aTf) into normal rats at early stages of development induces an increase in myelin formation and OLGc maturation as evaluated by different parameters (Escobar Cabrera et al., 1994, 1997; Paez et al., 2002). In ID rats, the immunoreactivity of mature OLGcs markers decreases significantly in comparison with normal controls, indicating a deficit in OLGc maturation (Badaracco et al., 2008). The intracranial injection of aTf reversed these changes.

Furthermore, with primary OLGc cultures from ID rats, we observed a high number of cells positive for the antibody against PSA-NCAM, whereas the number of myelin basic protein (MBP)-positive cells decreased compared with controls. Treatment with aTf reduced the population of PSA-NCAM-positive cells and increased the number of MBP-positive OLGcs. Based on these findings, the objective of this paper was to investigate the effects of iron deficiency during early development in rats on the cellular events occurring in the corpus callosum (CC) as well as the protective effects of an intracranial injection of aTf on oligodendrogenesis.

Results indicate that iron deficiency increases the number of proliferating and undifferentiated cells in the CC, suggesting alterations in oligodendrocyte maturation. Both myelin and axon integrity were analyzed by MBP and neurofilament-200 (NF-200) expression. MBP immunoreactivity in ID animals decreased, and NF-200-positive elements devoid of MBP reactivity were observed. A single injection of aTf at 3 days of age reverses the effect of iron deficiency, increasing the number of mature cells and myelin deposition.

MATERIALS AND METHODS

Materials

Paraformaldehyde, Hoechst 33258, Triton X-100, rat aTF, and 5-bromo-2′-deoxyurine (BrdU) were purchased from Sigma (St. Louis, MO). Anti-MBP antibody (rabbit) was a generous gift from Dr. A.T. Campagnoni (UCLA). Anti-PSA-NCAM antibody (mouse) was a generous gift from Dr. Rougon (Université de la Méditerranée-Marseille). Anti-NG2 antibody (rabbit) was obtained from Dr. J. Levine's laboratory. O4 antibody (mouse) was obtained from Chemicon (Temecula, CA); anti-Olig1 antibody (mouse) was purchased from Neuromics (Edina, MN). Anti-NF-200 (rabbit) was obtained from Sigma, and antiproliferating cell nuclear antigen (PCNA; mouse) was provided by Dako (Glostrup, Denmark). The secondary antibodies used were Cy3 donkey anti-rabbit, Cy3 goat anti-mouse, and Cy5 goat anti-rabbit from Jackson Immunoresearch (West Grove, PA) and Alexa Fluor 488 goat anti-mouse from Molecular Probes (Carlsbad, CA). Vectashield was used as mounting medium. All other chemicals were obtained from Sigma and were of the highest quality available.

Animal Model and Experimental Design

Pregnant Wistar dams were fed a control diet (40 mg Fe/kg) or an ID diet (4 mg Fe/kg) beginning at gestational day 5, according to Han et al. (2002). Diet containing low levels of iron was prepared at the Department of Nutrition (School of Pharmacy and Biochemistry) according to Harlan Teklad Nutritionals (Madison, WI). Pregnant dams and pups were maintained on their diets through out gestation and lactation. Rats had free access to food and water 24 hr/day. Lights were turned off between 7.00 PM and 7.00 AM, and room temperature was maintained at 25°C. The experimental protocol followed the *Principles of laboratory animals care* (NIH publication 85-23 revised 1985) and was approved by the Ethics Committee for Animal Research of the University of Buenos Aires.

At P3, pups were anesthetized with ethyl ether and perfused with 4% paraformaldehyde solution through the left heart ventricle (n = 16 for each group). In another set of experiments, control and ID rats were intracranially injected (ICI) at P3 with aTf (n = 16). The ICI of aTf or saline was carried out with animals under light ether anesthesia as previously described (Escobar Cabrera et al., 1994). For the injection, we used a 10-μl Hamilton syringe provided with a short-bevel No. 28 intradermal needle, custom-modified with a limiting epoxy resin drop placed on the outside of the cannula that prevented its penetration beyond 3 mm. The injection was done slightly above and between the eyes (Bregma) at a dose of 350 ng/brain in a volume of 5 μl. The solution was slowly injected to avoid overflows, and the syringe was not withdrawn until 1 min after being emptied. Control animals' ICIs with aTf were analyzed by monitoring the aTf effect (data not shown). ID animals ICI with 5 μl of saline solution at 3 days were used as ID controls (n = 16). Normal rats' ICIs with saline at 3 days of age were used as further controls (n = 16). At P11, the above-mentioned animals were anesthetized with ketamine/xilazine (75 mg/kg body weight and 10 mg/kg body weight, respectively) and were perfused through the left heart ventricle with 4% (w/v) paraformaldehyde solution. Animals for each group were randomly selected; body weight was measured, and blood samples were collected from the abdominal aorta for hematocrit determination.

Tissue Preparation

Brains were dissected out and sequentially placed in 4% paraformaldehyde (24 hr),15% sucrose (48 hr), and 30% sucrose (24 hr). Coronal and sagital sections (50 μm) were performed with a Leica CM 1850 Cryotome, and sections were kept in PBS:glycerine (1:1) solution.

BrdU Incorporation and Cell Counting

To evaluate cell proliferation, animals of each group were intraperitoneally injected with BrdU (80 mg/kg) once per day for 7 days starting at P4 and sacrificed at P11. Coronal sections (corresponding to plates 11–19 in Swanson's *Brain maps: structure of the rat brain*) were analyzed (see Fig. 4A, upper left). The CC was divided into different areas from 1 to 10 (see Fig. 4A, upper right). The medial CC was represented by areas 5 and 6 and the lateral CC by areas 1, 2, 3 and 8, 9, 10. $BrdU^+$ cells were counted in 1-mm by 1-mm squares (counting frame) using the Image-ProPlus 5.1 program. Counting frames were sampled five times at random, and an average value was obtained in each area of the nine coronal sections mentioned above over 16 animals (n = 144) for each experimental group. Enhancement contrasts were set to make a sharp image of positive nuclei, and the selected measured parametres were area (1–80,000 pixels) and aspect (1–100,000). With a ×20 objective, the number of cell nuclei intersecting the uppermost focal plane was expressed as 1) mean number of $BrdU^+$ cells/mm^2 and 2) percentage of $BrdU^+$ cells in each area.

Immunohistochemistry

Cryotome sections obtained as mentioned above were rinsed twice with PBS, 0.1% (v/v) Triton X-100 and then blocked for 2 hr with PBS containing 0.1% (v/v) Triton X-100 and 5% goat serum (GS). Sections used for BrdU immunohistochemistry were treated with 2 N HCl for 30 min at room temperature, followed by a thorough washing in 100 mM borate buffer, pH 8.5, prior to PBS 0.1% treatment and blocking. Incubations with primary antibodies were performed in PBS containing 0.1% (v/v) Triton X-100 and 1% (v/v) GS as follows: anti-BrdU (1:1,000), anti-MBP (1:400), anti-PSA-NCAM (1:100), anti-NG2 (1:200), O4 antibody (1:200), anti-Olig1 (1:100), anti-PCNA (1:200), and anti-NF-200 (1:200). Incubations were performed overnight at 4°C. Subsequently, all sections were placed for 2 hr at room temperature in the following secondary antibodies: Alexa Fluor 488 goat anti-mouse (1:400), Cy3 goat anti-rabbit (1:400), Cy3 donkey anti-mouse (1:400), and Cy5 goat anti-rabbit (1:400). No immunolabeling was detected in sections from control experiments, in which the primary antibodies were omitted. Double-immunostaining assays were performed using primary and secondary antibody cocktails. Sequential incubation steps were performed when the species of both primary antibodies were the same. In these cases, assays in which one of the primary antibodies was alternatively omitted were performed as controls. Microscopic observations were made with an Olympus BX50 epifluorescence microscope provided with a Cool-Snap digital camera. Images were analyzed in Image-ProPlus 5.1. Images of lateral areas (1–3 or 8–10) of the CC from all the experimental groups were used in order to quantify IHQ. Positive cells or integrated optical density (IOD) was measured, sampling counting frames at random five times for each image (n = 32). Image-ProPlus 5.1 settings were described above. Values are shown as mean positive cells/mm^2 or mean IOD/mm^2 and expressed as a percentage of control conditions. Hoechst stain was used as a cytological landmark for markers with nuclear localization (data not shown).

Perl's Stain for Detection of Ferric Iron

Sections were processed using a modification of the Perl's staining protocol to detect ferric iron (Moos and Mollgard, 1993; Bishop and Robinson, 2001). Briefly, sections were incubated for 30 min in 5% potassium ferrocyanide in PBS and 30 min in 5% potassium ferrocyanide + 1% (w/v) HCl in PBS and then washed for 20 min in PBS. Intensification of Perl's reaction was performed by incubating the sections for 15 min in DAB-Ni sulfate (3′-3′-diaminobenzidine-nickel sulfate) 0.05%:0.01% (w/v), followed by two 15-min incubations in DAB-Ni-sulfate + H_2O_2 (0.005%), and then washed three times with PBS for 20 min. The sections were mounted onto gelatinized slides, cleared in xylene, and coverslipped with Canada balsam (synthetic).

Confocal Microscopy

For the confocal analysis of tissue sections, an Olympus Fluoview FV1000MPE multiphoton laser scanning microscope was used to localize Cy3 goat anti-rabbit (543 nm laser-line excitation, 567/55 emission filter), and Cy5 goat anti-rabbit (647 excitation, 680/32 emission filter). Optical sections (Z = 0.5 μm) of confocal epifluorescence images were acquired using a Plan Apo ×60 oil objective (NA 1.42) with LaserSharp software (version 3.2; Bio-Rad, Hercules, CA). FV10-ASW 1.6 Viewer software was subsequently used to merge images and orthogonal studies, respectively. Merged images were processed in Photoshop 7.0 with minimal manipulations of contrast.

Electrophysiological Recordings

Visual evoked potentials (VEPs) were determined in control, control aTf, ID, and ID aTf rats (n = 4 for each group). Two electrodes were surgically placed into P16 rats. One was placed in the intersection between the midline of the skull and the line between the eyes and the other in the intersection between the midline of the skull and the occipital areas. Both electrodes were isolated and fixed with dental acrylic, and the skin was sutured with nylon 5/0. Five days after electrode implantation, VEP activity was assessed in dark-adapted rats as follows: after 6 hr of dark adaptation, rats were anesthetized with an intraperitoneal injection of ketamine/xilazine (50 mg/kg body weight and 0.5 mg/kg body weight, respectively) under dim red illumination. Phenylephrine hydrochloride (2.5%) and 1% tropicamide (Alcon Laboratories) were used to dilate the pupils, and the cornea was intermittently irrigated with balanced salt solution (Alcon Laboratories) to maintain the baseline recording and to prevent exposure keratopathy. All recordings were completed within 20 min of the induction of anaesthesia, and animals were kept warm during and after the procedure. Each eye was registered individually, occluding the contralateral eye, and a 70-stimuli average was taken. The stimuli were a full-field Ganzfeld with an unattenuated white light (5 msec, 1 Hz) from a photic stimulator (light-emitting diodes) set at maximum brightness (350 cd sec m^{-2} without a filter), amplified, filtered (0.5-Hz

TABLE I. Body Weight and Hematocrits in P11 Rats†

Experimental groups	Body weight (g)	Hematocrit value (%)
Co	30 ± 2.8	29 ± 1.0
ID	18.9 ± 0.1	9 ± 0.4★
ID aTf	19 ± 0.7	8.8 ± 1.7★

†Body weight expressed in grams and hematocrit as percentage. Data are shown as mean ± SEM. Co, control animals injected with saline; ID, iron-deficient animals injected with saline; ID aTf, iron-deficient rats injected with aTf; n = 4 for each group.
★$P < 0.05$ compared with control.

lowpass filter, 100-Hz highpass filter, notch activated), and averaged (Akonic BIO-PC). To analyze the registry, the amplitude (μV) of wave 4 was measured between the N2 deflection and the P2 peak. The latency (msec) of P2 was measured from the onset to the second positive peak (Halliday et al., 1972; Odom et al., 2004).

Statistical Analysis

Data from the various experimental groups were subjected to parametric tests suitable for normally distributed populations. One-way ANOVA was followed by Dunn's multiple comparison test and/or by Bonferroni's multiple-comparisons test. Statistical analysis between multiple groups was carried out using two-way ANOVA followed by Newnan-Keuls posttest with Graph Pad Prism 4.0 software.

RESULTS

Table I shows the values of body weight and hematocrit in ID and controls rat pups. Body weight at P11 in ID rats was significantly lower than in controls (about 60%), and hematocrit values were also lower in ID than in control rats (30% of controls values). These parameters did not return to normal values after the aTf treatment.

Iron Distribution in the CC

Using the Perl's staining reaction, we analyzed iron distribution in the CC of P11 animals, under different experimental conditions. For control animals, we detected numerous cells that stained prominently for iron staining. The majority of these cells were process bearing and showed the morphological characteristics of oligodendrocytes (Fig. 1A,B). Some were mostly process bearing, emanating up to four primary processes. Many of these cells were found to be oriented longitudinally within the CC, a distribution that characterizes oligodendrocytes. Under control conditions, some microglial cells are also positive for Perl's reaction. In the ID animals, iron staining was much less prominent, and cells were found to be transversally oriented, at variance with what was observed in control rats (Fig. 1C,D). Finally, in the CC of ID animals with ICI of aTf, the number of cells that stained prominently for iron was much higher than in ID animals. Many of these iron-containing cells were process bearing and were mostly oriented in longitudinal rows, showing the morphological features

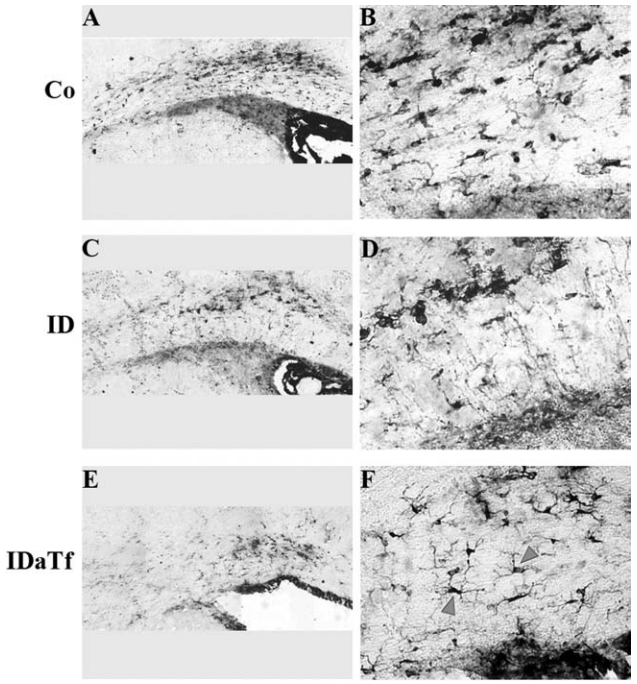

Fig. 1. Perl's staining of CC in P11 rats. Coronal sections from the CC. **A:** Control animals injected with saline (Co). **C:** ID rats injected with saline. **E:** ID rats injected with aTf (ID aTf). Magnification ×10. **B,D,F:** Higher magnifications (×20) of A, C and E, respectively. Arrowheads show iron-stained cells with a phenotype of mature oligodendrocyte.

of mature OLGcs (Fig. 1E,F, arrowheads). Perl's staining for cells with an activated microglia phenotype was not observed. These results are in accordance with those in ID rats with and without aTf treatment, in which activated microglia were not observed (data not shown).

At P3, Most of the PCNA-Positive Cells Were Undifferentiated OLGcs

The OLGc population in control and ID rats at P3 was analyzed by immunohistochemistry in sections of the CC using anti-PCNA, anti-Olig1, and O4 antibodies (Figs. 2, 3). PCNA-positive cells, actively proliferating, were detected in both groups of animals. Olig-1 immunoreactivity, used as a marker of OPCs (Fig. 2E), was higher (26%; $P < 0.05$) in ID rats than in controls. By double immunostaining, the number of PCNA/Olig-1-positive cells was found to be higher in the ID group ($P < 0.05$). Moreover, in ID animals, most of the PCNA-positive cells were also Olig-1 positive (66%; Fig. 2F). The levels of O4-positive cells (marker of oligodendroglial linage) were significantly higher (46%; $P < 0.001$) in ID rats compared with controls (Fig. 3E), and merged images (PCNA/O4) showed that most of the $PCNA^+$ cells were also O4 positive (80%; Fig. 3F). At this stage, Rip (oligodendrocytes marker) and MBP immunoreactivity was negative (data not shown).

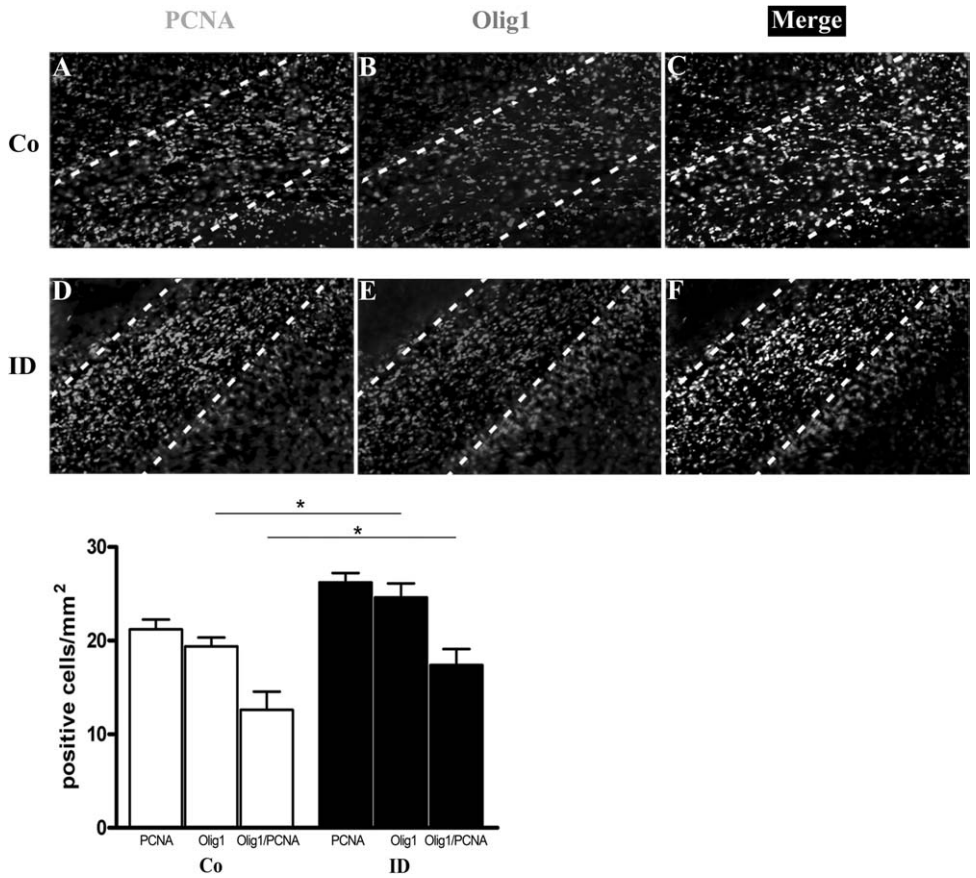

Fig. 2. Distribution of PCNA- and Olig-1-positive cells in coronal sections of CC in P3 rats. **A,D:** Antiproliferating cell nuclear antigen-positive cells ($PCNA^+$) in Co and ID animals, respectively. **B,E:** Olig-1^+ cells in Co and ID animals. **C,F:** Overlay of PCNA- and Olig-1-positive cells (white) in Co and ID groups. The overlay shows that a large proportion of $PCNA^+$ cells is also Olig-1^+ cells in the ID group. White dashed lines show the boundaries of the CC. Abbreviations as in Figure 1. The quantification of each marker was done as described in Materials and Methods. Results are expressed as mean (positive cells/mm^2) ± SEM. Asterisks indicate significance ($^*P < 0.05$). Magnification ×20.

The Distribution of BrdU-Positive Cells in the Corpus Callosum Is Different in Control and ID Animals

Quantitative analysis and distribution of $BrdU^+$ cells in the CC for the different treatment groups at 11 days of age is shown in Figure 4. The total number of $BrdU^+$ cells, determined in a row of nine tissue sections (left upper panel and see also Materials and Methods) increased in ID rats and returned to control values in the ID animals injected with aTf. The average number of $BrdU^+$ cells (mean/mm^2) was 57.3 ± 1.5, 41.5 ± 1.6, and 45.1 ± 1.5 for the ID, Co, and aTf-treated ID rats, respectively (Fig. 4A). To analyze the distribution of this cell population, each section was evaluated following the procedures described above (see Fig. 4A, upper right panel). The percentage distribution of $BrdU^+$ cells in each area was calculated by adding the number of $BrdU^+$ cells present in similar areas of all the sections (Fig. 4B–D). The distribution pattern of these cells in different areas varied among the various experimental groups. In the control group, there were significant differences between areas 5 and 6 compared with areas 1, 2, 3, and 8, 9, 10 (Fig. 4B, Table II). A distribution pattern similar to that of controls was observed in the ID aTf group (Fig. 4D, Table II). On the other hand, the distribution pattern of $BrdU^+$ cells in the ID animals was quite uniform among the various areas (Fig. 4C, Table II). It was noticed that the percentage of $BrdU^+$ cells in areas 5 and 6 was higher in the ID group (Fig. 4C, left image) in comparison with both Co (Fig. 4B, left image) and ID aTf groups (Fig. 4D, left image). Although areas 1–3 and 8–10 in ID rats seem to show percentages of $BrdU^+$ cells similar to those observed in Co and ID aTf, it should be recalled that they actually represent values obtained from an increased $BrdU^+$ total cell population, as shown in Figure 4A.

At P11, Most of the $BrdU^+$ Cells in ID Animals Remained as OPCs

The maturation stage attained by $BrdU^+$ cells along the oligodendrocyte differentiation process was analyzed with anti-NG2 and anti Olig-1 as markers of

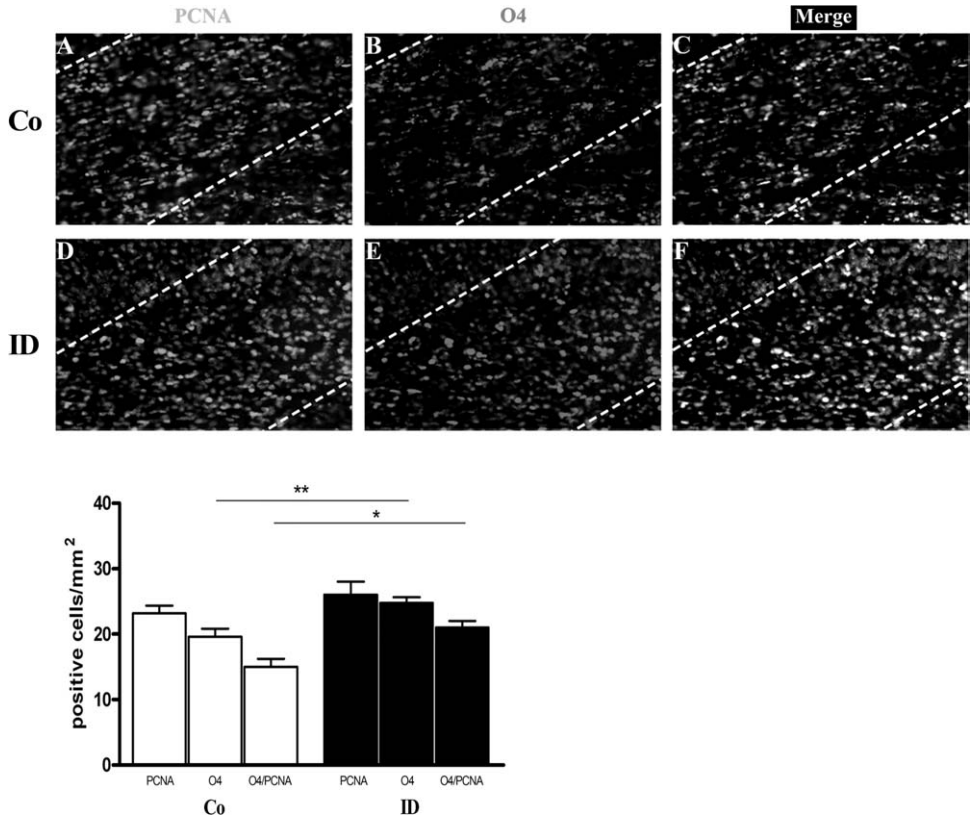

Fig. 3. Distribution of PCNA- and O4-positive cells in coronal sections of CC in P3 rats. **A,D:** Antiproliferating cell nuclear antigen-positive cells ($PCNA^+$) in Co and ID animals, respectively. **B,E:** $O4^+$ cells in Co and ID animals, respectively. **C,F:** Overlay of PCNA and O4 positive cells (white) in Co and ID groups, respectively. The overlay shows that a large proportion of $PCNA^+$ cells is also $O4^+$ cells in the ID group. White dashed lines show the boundaries of the CC. Abbreviations as in Figure 1. Quantification of each marker was done as described in Materials and Methods and is expressed as mean (positive cells/mm^2) ± SEM. Significant differences are indicated by asterisks ($\star P < 0.05$, $\star\star P < 0.01$). Magnification ×20.

undifferentiated precursors and OPCs, respectively (Figs. 5, 6). The average number of NG2-positive cells (mean/mm^2) was significantly higher in ID animals compared with controls (37.20 ± 2.38 and 22.2 ± 8.07, respectively; $P < 0.01$; Fig. 5E). The amount of BrdU-labeled cells that were also NG2 immunopositive was greater in ID animals than in controls (146%; $P < 0.001$), suggesting that at this stage a large amount of the BrdU-positive cell population has not yet reached a mature oligodendroglial cell phenotype (Fig. 5F). Similar results were obtained by analyzing the Olig-1-positive cells (Fig. 6), confirming that the largest part of the cells in ID animals were at the stage of OPCs (Fig. 6E). The same determinations were carried out in P11 ID animals intracranially injected at 3 days of age with a single dose of aTf. In this case, results showed that the amount of Olig-1-positive cells was reduced in aTf-treated animals (Fig. 6H).

To evaluate cells in the process of active migration, we analyzed cells expressing PSA-NCAM (Menn et al., 2006; Fig. 7). The profile of migrating cells was significantly higher in the CC of ID rats compared with controls (Fig. 7B). In ID rats treated with aTf, the PSA-NCAM immunoreactivity was significantly lower than in ID rats (Fig. 7C).

Immunolabeling with O4 antibodies showed a decrease in O4 immunoreactivity in the ID group compared with control animals. Immunoreactivity increased markedly after the ICI of aTf (Fig. 8A). In agreement with previous studies from our laboratory (Badaracco et al., 2008), MBP immunohistochemistry showed that there was a marked hypomyelination in the CC in the ID group. After aTf treatment, ID animals showed an increase in myelin deposition as revealed by a marked increase in MBP immunoreactivity (Fig. 8B). To analyze further the effect of neonatal iron deficiency on both myelin and axon integrity, we analyzed MBP and NF-200 expressions in brain coronal sections of the CC by confocal microscopy. In control animals, the close association between immunoreactivity was evident; positive immunoreactivity for NF-200, limited by MBP-positive structures, was detected in the longitudinal sections of myelinated axons (arrowheads) and, particularly, in cross-sections in which NF-200-positive elements

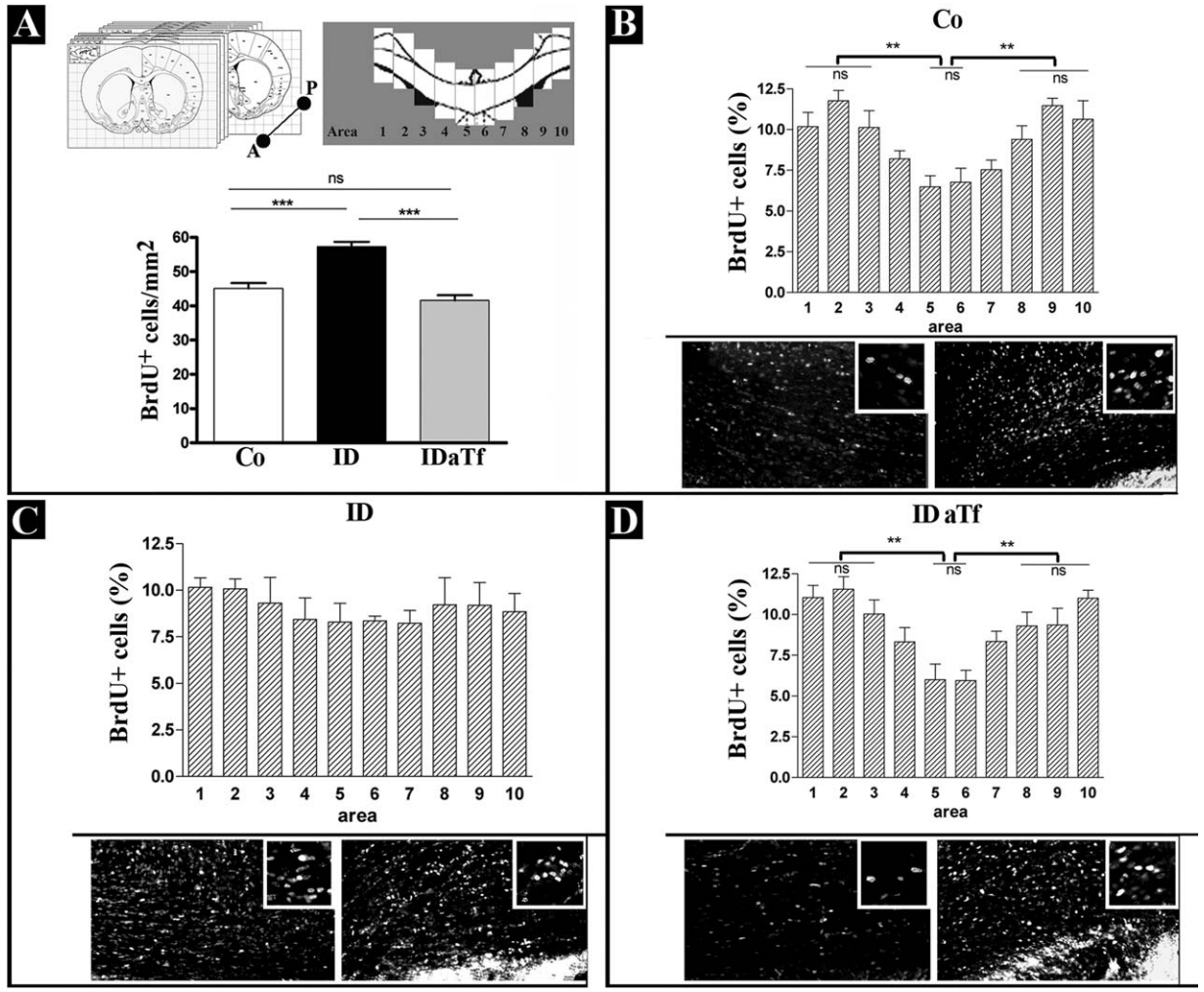

Fig. 4. Quantitative analysis and distribution of $BrdU^+$ cells in the CC of P11 rats. The CC was divided into 10 areas (upper right representation). The medial CC corresponds to areas 5 and 6, whereas the lateral CC corresponds to areas 1, 2, 3, 8, 9, and 10. **A:** $BrdU^+$ cells were counted in the CC over nine successive coronal sections on the A-P axis (upper left representation). Bars show the number of $BrdU^+$ cells (mean/mm^2 ± SEM) for each experimental group. Distribution of the $BrdU^+$ cells is expressed as the percentage of cells in different areas of the CC for controls (**B**), ID (**C**), and ID aTf (**D**). Representative darkfield images of medial CC (left) and lateral CC (right) of each group are shown. Magnification ×20. **Insets:** ×40. Abbreviations as in Figure 1. Quantification of $BrdU^+$ cells was done as described in Materials and Method. Significant differences are indicated by asterisks (**$P < 0.01$, ***$P < 0.001$; ns, not significant).

surrounded by MBP immunoreactivity were clearly observed (Fig. 9, white arrows). A decreased MBP immunoreactivity in ID animals was clearly detected, and NF-200-positive elements devoid of MBP-positive reactivity were visualized in ID animals (Fig. 9, black arrows). The close association between these two markers was reestablished in ID animals that had been treated with aTf. Assuming that the hypomyelination observed in the CC of ID animals could also affect, among other brain structures, the optic pathway, we analyzed its functional integrity exploring extracellular visual evoked potentials (VEPs) in the different experimental groups, as described in Materials and Methods. Latency, an electrophysiological parameter that indicates a slower speed of conduction and that is generally considered as being associated with myelin integrity, increased significantly in ID rats in comparison with controls (134.85 ± 4.3 msec and 112.6 ± 1.64 msec, respectively), indicating defective myelin or hypomyelination. Amplitude, on the other hand, a parameter that is considered to be related to the number and integrity of the nerve fibers, decreased significantly in the ID animals compared with the control group (14.72 ± 7.52 μV and 30.60 ± 7.70 μV, respectively). Both amplitude and latency were affected, which suggests that the integrity of the nerve fiber was also damaged in association with hypomyelination. Both values were substantially normalized in the animals that were treated

TABLE II. Percentage of BrdU$^+$ Cells in Different Areas of the CC⋆

	Areas									
Experimental groups	1	2	3	4	5	6	7	8	9	10
Co	10.2 ± 0.9	11.8 ± 0.6	10.2 ± 1.0	8.2 ± 0.5	6.5 ± 0.7	6.8 ± 0.9	7.5 ± 0.6	9.4 ± 0.8	11.5 ± 0.5	10.6 ± 1.1
ID	10.2 ± 0.5	10.1 ± 0.5	9.3 ± 1.4	8.4 ± 1.2	8.3 ± 1.0	8.3 ± 0.3	8.2 ± 0.7	9.2 ± 1.4	9.2 ± 1.2	8.8 ± 1.0
ID aTf	11.0 ± 0.8	11.6 ± 0.8	10.0 ± 0.9	8.3 ± 0.9	6.0 ± 1.0	6.0 ± 0.6	8.4 ± 0.6	9.5 ± 0.9	9.4 ± 1.0	11.0 ± 0.5

⋆Each value is expressed as the percentage of BrdU$^+$ cells in the same area of nine different coronal sections over 16 animals (n = 144). Co, control animals injected with saline; ID, iron-deficient animals injected with saline; ID aTf, iron-deficient rats injected with aTf.

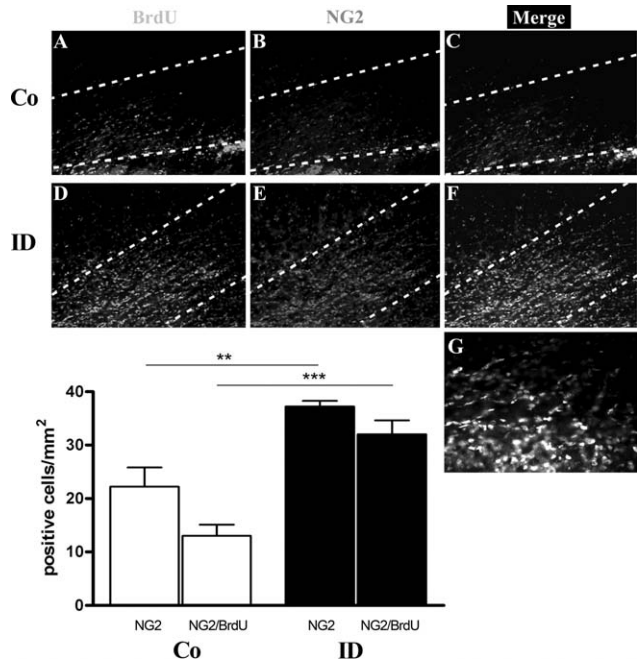

Fig. 5. NG2-positive cells in coronal sections of the CC in P11 rats. **A,D:** BrdU$^+$ cells in Co and ID animals, respectively. **B,E:** NG2$^+$ cells in Co and ID animals, respectively. **C,F:** Overlay of BrdU and NG2 positive cells (white) in Co and ID groups, respectively. **G:** Higher magnifications (×40) of F; the localization of the NG2 label depicts nonendothelial morphology. The overlay shows that a large proportion of BrdU$^+$ cells is also NG2$^+$ in the ID group. White dashed lines show the boundaries of the CC. Abbreviations as in Figure 1. Quantification of each marker was performed as described in Materials and Methods and is expressed as mean (positive cells/mm^2) ± SEM. Significant differences are indicated by asterisks (⋆⋆$P < 0.01$, ⋆⋆⋆$P < 0.001$). Magnification ×20.

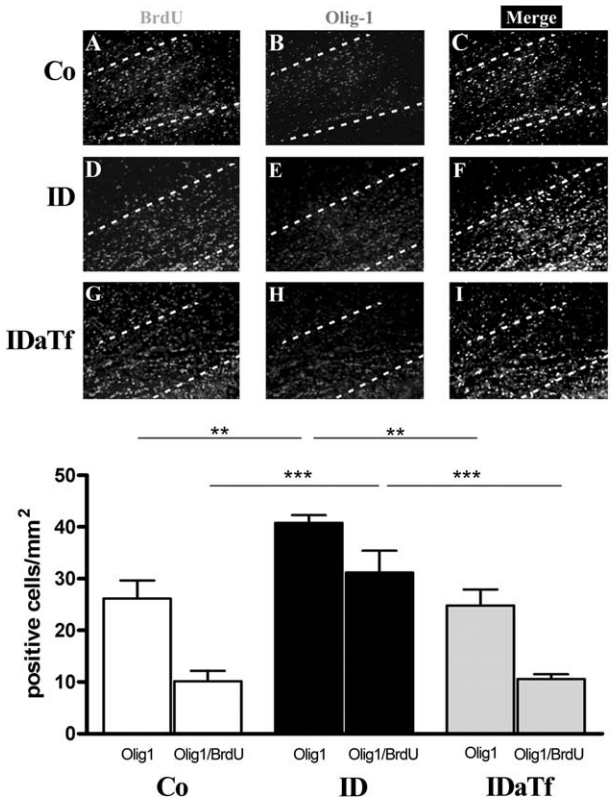

Fig. 6. Characterization of OPCs in coronal sections of the CC in P11 rats: Effect of aTf. **A,D,G:** BrdU$^+$ cells in Co, ID, and ID aTf, animals respectively. **B,E,H:** Olig-1$^+$ cells in Co, ID, and ID aTf animals, respectively. **C,F,I:** Overlay of BrdU- and Olig-1-positive cells in Co, ID, and ID aTf groups, respectively. The overlay shows that a large proportion of BrdU$^+$ cells is also Olig-1$^+$ cells in the ID group. White dashed lines show the boundaries of the CC. Abbreviations as in Figure 1. Quantification of each marker was done as described in Materials and Methods and is expressed as mean (positive cells/mm^2) ± SEM. Significant differences are indicated by asterisks (⋆⋆$P < 0.01$, ⋆⋆⋆$P < 0.001$). Magnification ×20.

with aTf (latency 113.4 ± 7.60 msec, amplitude 25.27 ± 3.70 μV).

DISCUSSION

Iron availability has been shown to affect the myelination processes, and iron deficiency in rats results in hypomyelination (Yu et al., 1986; Ortiz et al., 2004). Oligodendrocyte stain for iron more robustly than any other cell in the normal adult brain (Connor and Menzies, 1990; Benkovic and Connor, 1993), and iron-positive cells, which most likely represent oligodendrocytes, have been found almost exclusively in white matter tracts in areas of myelinogenic foci (Connor and Menzies, 1996). Under normal conditions, iron accumulates in oligodendrocytes when these cells are able to mature and produce myelin (Taylor and Morgan, 1990;

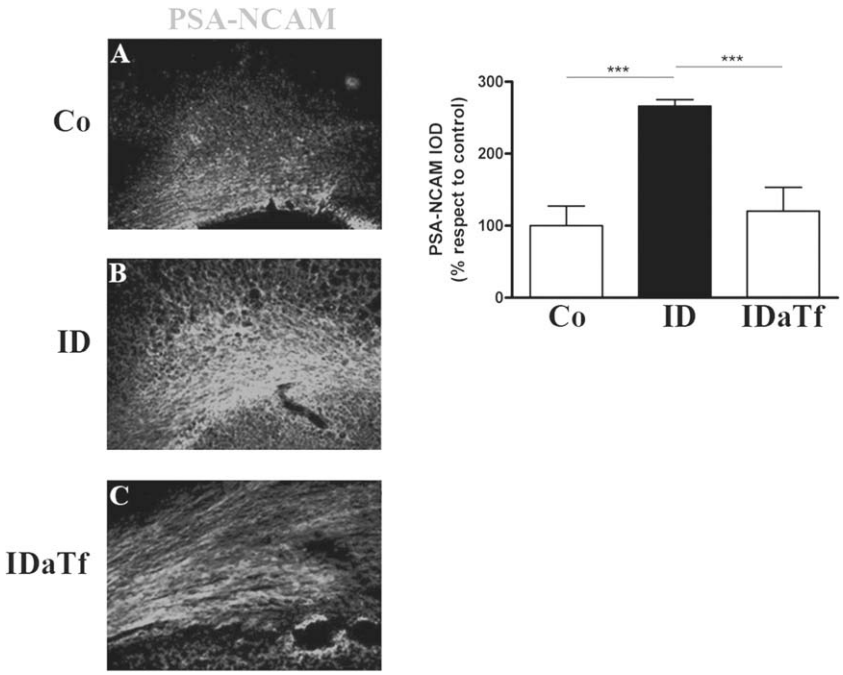

Fig. 7. IOD of PSA-NCAM in coronal sections of the CC in P11 rats. **A–C:** PSA-NCAM$^+$ cells in Co, ID, and ID aTf groups, respectively. Abbreviations as in Figure 1. Quantification of each marker was done as described in Materials and Methods. Mean IOD/mm^2 is expressed as a percentage of control conditions. Significant differences are indicated by asterisks (***$P < 0.001$). Magnification ×10.

LeVine, 1991; Connor and Menzies, 1996), but it is not clear whether this iron accumulation is required for the maturation of oligodendrocytes or if it is just a site of brain iron storage. Within this context, it has been shown that iron availability modulates the generation of oligodendrocytes from precursor cells (Morath and Mayer-Pröschel, 2001). It is well documented that iron is an important cofactor for correct synthesis of the myelin membrane (Kwik-Uribe et al., 2000).

In vitro studies from our laboratories, in which OLGcs were cultured under specific conditions for studying the effects of iron deprivation on their differentiation, showed that in ID animals there was a decreased number of differentiated OLGcs relative to controls. In cultured OLGcs isolated from ID rats treated with aTf, the number of MBP-positive cells was increased and the number of PSA-NCAM-positive cells was decreased (Badaracco et al., 2008).

In the present study, we investigated the behavior of OLG precursor cells in rats subjected to an ID diet from gestational day 5 and the effect of a single ICI of aTf on the process of maturation of this myelin-forming cell. The investigation was performed at P3 and P11. We have previously described a temporal window of aTf effects (Marta et al., 2000), showing that aTf induces an increased maturation of the OLGc precursors when the ICI of aTf is performed at P3. This finding led us to characterize the cell population at P3, which was the first point of our study. At this early age, the relative amount of PCNA-positive cells showed a tendency to increase in ID compared with controls. The population of doubly marked cells, PCNA/Olig1 or PCNA/O4, in ID animals also increased, indicating that most of the PCNA-positive cells were in an undifferentiated state compared with controls, because OPCs (Olig1$^+$ cells) and pre-OLGc (O4$^+$ cells) actively proliferate (Fok-Seang and Miller, 1994). O4 immunolabeling at P3 almost exclusively corresponds to immature stages of the oligodendrocyte lineage given that MBP and Rip immunoreactivity was undetectable at this stage. These results suggest that the availability of undifferentiated precursors was higher in the ID group. The OLGc precursors seem to be unable to transit along the different OLGc maturation stages beyond the OPC level, and, as a consequence, they could not synthesize a normal and mature myelin. These results agree with those of Morath and Mayer Pröschel (2001), who described that iron deficiency during pregnancy affects the iron levels of brain in the developing fetus and not only disrupts the proliferation but also disturbs the generation of oligodendrocytes from these precursor cells.

Studies at P11 involved the immunohistochemical analysis of cell proliferation using BrdU labeling, a characterization of OLGcs and their precursors, and an analysis of their dynamics. Long-term BrdU experiments (seven pulses for 7 days) were chosen to evaluate the accumulation of proliferating cells in a developmental window.

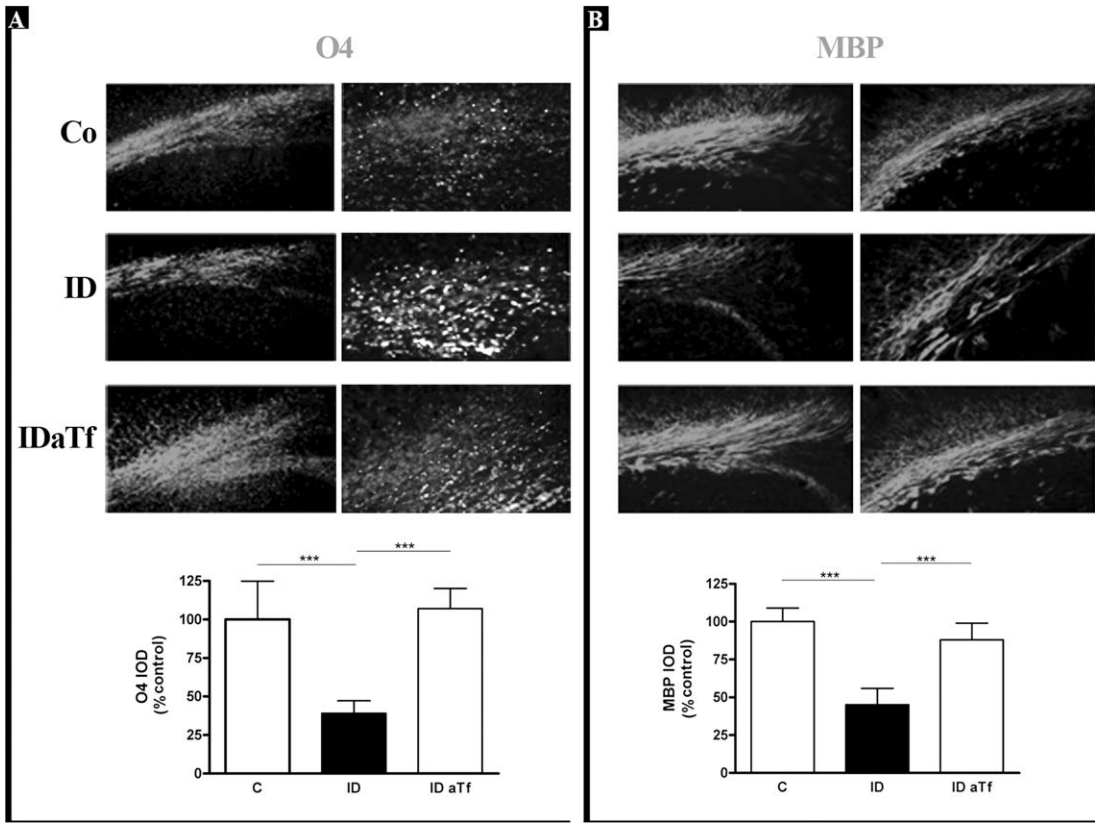

Fig. 8. Characterization of OLGcs with O4 and anti-MBP antibody in coronal sections of the CC in P11 rats. **A:** $O4^+$ cells in Co, ID, and ID aTf groups. Left panels: magnification ×10. Right panels: magnification ×20. White label: $BrdU^+$ cells. **B:** MBP immunoreactivity in Co, ID, and ID aTf groups (magnification ×10). Left panels: medial-lateral areas of the CC. Right panels: lateral areas of the CC. Abbreviations as in Figure 1. Quantification of each marker was done as described in Materials and Methods. Mean IOD/mm^2 is expressed as a percentage of control conditions. Significant differences are indicated by asterisks (***$P < 0.001$). IOD values show no significant differences between Co and ID aTf animals.

The cell population at P11 showed that the $BrdU^+$ cells increased in ID animals compared with controls. When ID rats were treated with aTf, a reduction of the cell proliferating population was observed. In coincidence with our results, Morath and Mayer Pröschel (2001) have demonstrated that at E 13.5 there is a slight, but not statistically significant, increase in the proportion of $BrdU^+/A2B5^+$ cells in cultures of purified glial restricted precursors isolated from the spinal cord. Also in coincidence with our results, Gazitt et al. (2001) observed that in HL-60 cells iron deprivation blocks phorbol myristate acetate (PMA)-induced differentiation of these cells by inhibiting the expression of the cell cyclin-dependent kinase inhibitor p21 and releasing cells from the G1/S cell cycle checkpoint.

The CC is a relatively simple structure composed of transversely aligned axon bundles in which the direction of progenitor migration appears to correspond exactly to that of the axon bundles that are still unmyelinated. In the ID rats, the distribution of BrdU-labeled cells was uniform along all the CC, whereas, in controls and ID intracranially injected with aTf, the progenitor cells were less concentrated in the middle area of the CC. Furthermore, $PSA\text{-}NCAM^+$ progenitor cells were more abundant, the increase of this cell population in the ID rats could explain their migration behavior. With reference to the increased reactivity for PSA-NCAM, it should be mentioned that it could represent a lack of down-regulation that has been shown to be a prerequisite for an efficient myelination by mature oligodendrocytes. It is possible that, in ID rats ICI with aTf, some of the progenitors could differentiate before reaching the midline of the CC, insofar as it was demonstrated that aTf inhibits cell migration by a process mediated by aTfR (Paez et al., 2002). Our results suggest that a single ICI of aTf at 3 days of age in ID rats causes a reversion of the defective OLGc maturation associated with ID, insofar as most of the OLGcs no longer had a migrating profile and showed immunoreaction against markers for mature cells.

To analyze the maturation stages attained by $BrdU^+$ cells, we characterized this cell population using different markers from early stages (anti-NG2, anti-Olig-1, and O4 antibody) up to markers of mature OLGcs,

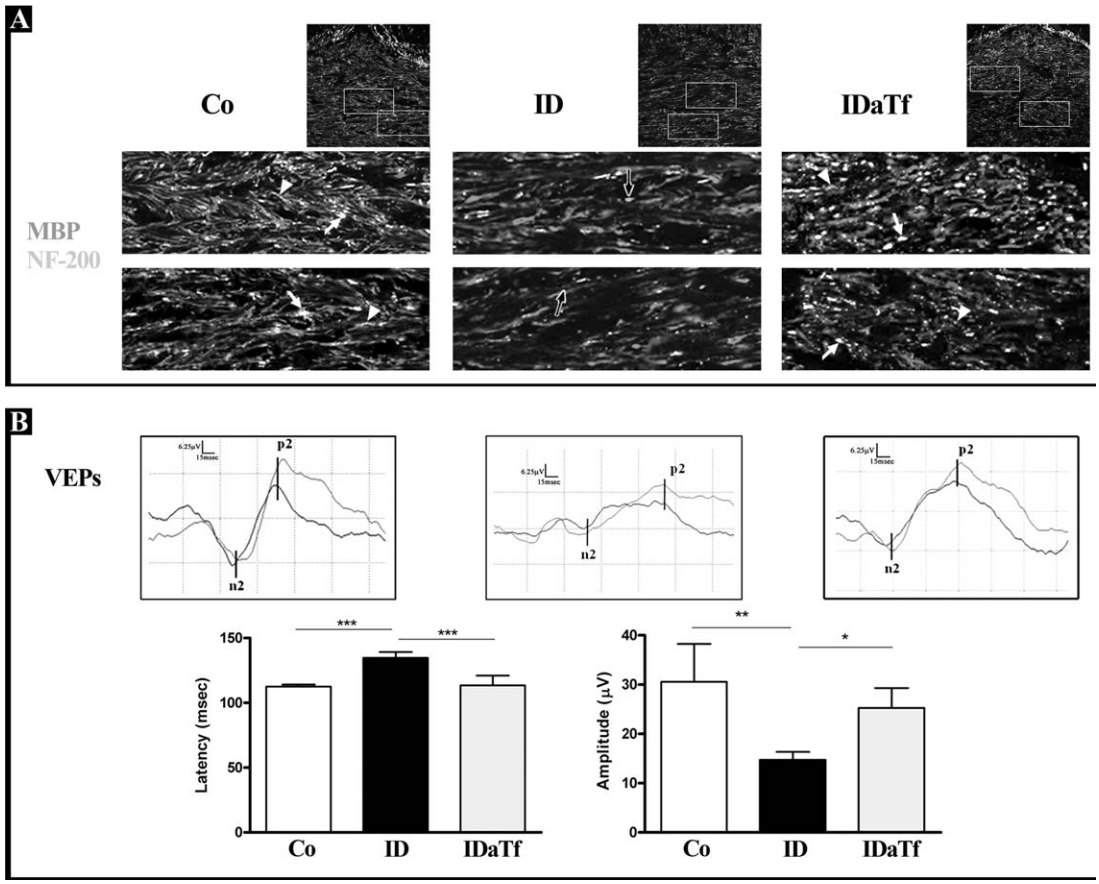

Fig. 9. aTf injection enhances axonal remyelination in hypomyelinated iron-deficient animals. Confocal images of the CC at P11 showing double immunolabeling with antibodies to MBP and NF-200. **A:** Representative images of Co, ID, and ID aTf animals. ×60 images; boxed areas are shown at higher magnifications in the lower panel. Longitudinal sections of axon fibers (NF-200 positive) show close association with MBP-positive structures (white dots on a row; white arrowheads). Transverse sections of NF-200-positive elements surrounded by MBP-immunoreactive structures (white dots; white arrows). NF-200-positive elements devoid of MBP-positive reactivity (grey dots on a single row or single dot; black arrows). **B:** VEPs in Co, ID, and ID aTf groups. Upper panels show representative registers. The amplitude (microvolts) was measured between the N2 deflection and the P2 peak. The latency (msec) of P2 was measured from the onset to the second positive peak. Abbreviations as in Figure 1. Quantification was done as described in Materials and Methods and is shown as mean ± SEM of at least three independent experiments. Each of them was done in triplicate. Significant differences are indicated by asterisks ($\star P < 0.05$, $\star\star P < 0.01$, $\star\star\star P < 0.001$).

such as anti-MBP and anti-Rip antibodies. O4 immunoreactivity at P11 [measured as integrated optical density (IOD)/mm^2] showed a complex situation. Given that O4 is a marker of different maturational stages of the OLGcs (from pre-OLGc to mature OLGc; Back et al., 2007; Mela and Goldman, 2009), in ID rats the majority of the label corresponds to the OPCs population, in that these cells failed to make progress to a more mature stage. On the contrary, in Co and ID aTf animals, O4 label corresponds not only to cells that remain as OPCs but also to mature stages of the linage. This is the reason why immunoreativity of O4 increased in Co and ID aTf and diminished dramatically at P11 in the ID group. When the distribution pattern of PSA-NCAM$^+$ cells was studied, the results indicated that these migrating cells were appreciably more numerous in the iron-deprived animals. At variance with these results in the ID rats ICI with a single dose of aTf, cells displayed a more mature phenotype.

Bartlett et al. (1991) demonstrated that, in myelin-deficient rats, in which oligodendrocytes fail to mature, levels of brain transferrin mRNA are below normal. These data demonstrate that oligodendrocytes and the iron-regulatory system in the brain are closely linked. Our results show that, after aTf injection, there is an increase only in OLGc maturation, and no correction in the levels of iron as evaluated by Perl's reaction was observed (Fig 1). This indicates that the effect of aTf does not seem to occur in the transport of iron into the brain but only in the maturation of the OLGcs. Given the strong iron staining of mature oligodendrocytes (Connor et al., 1995; Connor and Menzies, 1996) and the clear role of iron in the myelination process, the lack of the traditional transferrin-mediated uptake system

indicates that there must be an uptake system for iron in oligodendrocytes that is independent of Tf.

Connor's group previously demonstrated that H-ferritin binds to white matter tracts in human and rodent brains (Hulet et al., 1999a,b, 2000) and that the spatial and temporal pattern of H-ferritin binding in the white matter of the CNS during development coincides with the onset of myelination (Hulet et al., 2002). More recently, T-cell immunoglobulin and mucin-domain-containing protein-2 (Tim-2) were shown to bind and internalize H-ferritin. Todorich et al. (2008) have clearly showed that Tim-2 is expressed in oligodendrocytes both in vivo and in vitro, providing compelling evidence that Tim-2 is the H-ferritin receptor in oligodendrocytes.

As a consequence of enhanced oligodendrogenesis but decreased maturation with iron deficiency, the number of myelinated axons present at P11 is lower, as evaluated by a double immunostaining with anti-MBP and -NF-200 antibodies. After a single ICI of aTf, the number of myelinated axons returned to control values. The optic nerve is an important structure rich in oligodendrocytes, which can be affected by ID, so we compared the immunohistochemical observations with electrophysiological measurements. VEP recording show a defective response to visual stimuli in ID animals compared with control rats. When ID animals were ICI with aTf, the optic nerve response to the visual stimuli became similar to that of controls.

These results support the hypothesis that iron deficiency increases the number of proliferating and undifferentiated cells in the CC. A hallmark of this study is the finding that a single injection of aTf reverses the effects of iron deficiency, increasing the number of mature cells and the deposition of myelin. ID animals exhibit an enlarged migrating, undifferentiated cell subpopulation with a limited capacity to progress beyond the precursor stage, whereas the OPC population recovers the capacity to mature and myelinate upon aTf treatment. These results reinforce the hypothesis that aTf acts by triggering OLGc differentiation and, as a consequence, promoting myelin repair.

ACKNOWLEDGMENTS

The participation of Dr. Pablo Sande from the Laboratorio de Neuroquímica Retiniana y Oftalmología Experimental, Departamento de Bioquímica Humana, Facultad de Medicina, Universidad de Buenos Aires and CEFyBO-Universidad de Buenos Aires-CONICET in the determination of VEPs is greatly acknowledged. We also thank Dr. Patricia Oteiza for discussion and editing of the manuscript.

REFERENCES

Badaracco ME, Ortiz EH, Soto EF, Connor J, Pasquini JM. 2008. Effect of transferrin on hypomyelination induced by iron deficiency. J Neurosci Res 86:2663–2673.

Back SA, Craig A, Kayton RJ, Luo NL, Meshul CK, Allcock N, Fern R. 2007. Hypoxia–ischemia preferentially triggers glutamate depletion from oligodendroglia and axons in perinatal cerebral white matter. J Cereb Blood Flow Metab 27:334–347.

Bamberg R. 2008. Occurrence and detection of iron-deficiency anemia in infants and toddlers. Clin Lab Sci 21:225–231.

Bartlett WP, Li X-S, Connor JR. 1991. Expression of transferrin mRNA in the CNS of normal and jimpy mice. J Neurochem 57:318–322.

Beard JL, Wiesinger JA, Connor JR. 2003. Pre- and postweaning iron deficiency alters myelination in Sprague-Dawley rats. Dev Neurosci 25:308–315.

Benkovic SA, Connor JR. 1993. Ferritin, transferrin, and iron in selected regions of the adult and aged rat brain. J Comp Neurol 338:97–113.

Bishop GM, Robinson SR. 2001. Quantitative analysis of cell death and ferritin expression in response to cortical iron: implications for hypoxia–ischemia and stroke. Brain Res 907:175–187.

Connor JR, Menzies SL. 1990. Altered cellular distribution of iron in the central nervous system of myelin deficient rats. Neuroscience 34:265–271.

Connor JR, Menzies SL. 1996. Relationship of iron to oligodendrocytes and myelination. Glia 17:83–93.

Connor JR, Pavlick G, Karli D, Menzies SL, Palmer C. 1995. A histochemical study of iron-positive cells in the developing rat brain. J Comp Neurol 355:111–123.

Dobbing J. 1990. Boyd Orr memorial lecture. Early nutrition and later achievement. Proc Nutr Soc 49:103–118.

Escobar Cabrera OE, Bongarzone ER, Soto EF, Pasquini JM. 1994. Single intracranial injection of apotransferrin in young rats induces increased myelination. Dev Neurosci 16:248–254.

Escobar Cabrera OE, Zakin MM, Soto EF, Pasquini JM. 1997. Single intracranial injection of apotransferrin in young rats increases the expression of specific myelin protein mRNA. J Neurosci Res 47:603–608.

Fok-Seang J, Miller RH. 1994. Distribution and differentiation of A2B5 glial precursors in the developing rat spinal cord. J Neurosci Res 37:219–235.

Franco PG, Silvestroff L, Soto EF, Pasquini JM. 2008. Thyroid hormones promote differentiation of oligodendrocyte progenitor cells and improve remyelination after cuprizone-induced demyelination. Exp Neurol 212:458–467.

Gazitt Y, Reddy SV, Alcantara O, Yang J, Boldt DH. 2001. A new molecular role for iron in regulation of cell cycling and differentiation of HL-60 human leukemia cells: iron is required for transcription of p21(WAF1/CIP1) in cells induced by phorbol myristate acetate. J Cell Physiol 187:124–135.

Greenwood K, Butt AM. 2003. Evidence that perinatal and adult NG2-glia are not conventional oligodendrocyte progenitors and do not depend on axons for their survival. Mol Cell Neurosci 23:544–558.

Halliday AM, McDonald WI, Mushin J. 1972. Delayed visual evoked response in optic neuritis. Lancet 1:982–985.

Han J, Day JR, Connor JR, Beard JL. 2002. H and L ferritin subunit mRNA expression differs in brains of control and iron-deficient rats. J Nutr 132:2769–2774.

Hulet SW, Powers S, Connor JR. 1999a. Distribution of transferrin and ferritin binding in normal and multiple sclerotic human brains. J Neurol Sci 165:48–55.

Hulet SW, Hess EJ, Debinski W, Arosio P, Bruce K, Powers S, Connor JR. 1999b. Characterization and distribution of ferritin binding sites in the adult mouse brain. J Neurochem 72:868–874.

Hulet SW, Heyliger SO, Powers S, Connor JR. 2000. Oligodendrocyte progenitor cells internalize ferritin via clathrin-dependent receptor mediated endocytosis. J Neurosci Res 61:52–60.

Hulet SW, Menzies S, Connor JR. 2002. Ferritin binding in the developing mouse brain follows a pattern similar to myelination and is unaffected by the jimpy mutation. Dev Neurosci 24:208–213.

Kwik-Uribe CL, Gietzen D, German JB, Golub MS, Keen CL. 2000. Chronic marginal iron intakes during early development in mice result

in persistent changes in dopamine metabolism and myelin composition. J Nutr 130:2821–2830.

Levine JM, Nishiyama A. 1996. The NG2 chondroitin sulfate proteoglycan: a multifunctional proteoglycan associated with immature cells [review]. Perspect Dev Neurobiol 3:245–259.

LeVine SM. 1991. Oligodendrocytes and myelin sheaths in normal, quaking and shiverer brains are enriched in iron. J Neurosci Res 29:413–419.

Marta CB, Escobar Cabrera OE, Garcia CI, Villar MJ, Pasquini JM, Soto EF. 2000. Oligodendroglial cell differentiation in rat brain is accelerated by the intracranial injection of apotransferrin. Cell Mol Biol 46:529–539.

Mela A, Goldman JE. 2009. The tetraspanin KAI1/CD82 is expressed by late-linage oligodendrocyte precursors and may function to restrict precursor migration and promote oligodendrocyte differentiation and myelination. J Neurosci 29:11172–11181.

Menn B, Garcia-Verdugo JM, Yaschine C, Gonzalez-Perez O, Rowitch D, Alvarez-Buylla A. 2006. Origin of oligodendrocytes in the subventricular zone of the adult brain. J Neurosci 26:7907–7918.

Moos T, Mollgard K. 1993. A sensitive post-DAB enhancement technique for demonstration of iron in the central nervous system. Histochemistry 99:471–475.

Morath DJ, Mayer-Pröschel M. 2001. Iron modulates the differentiation of a distinct population of glial precursor cells into oligodendrocytes. Dev Biol 237:232–243.

Morath DJ, Mayer-Pröschel M. 2002. Iron deficiency during embryogenesis and consequences for oligodendrocyte generation in vivo. Dev Neurosci 24:197–207.

Odom JV, Bach M, Barber C, Brigell M, Marmor MF, Tormene AP, Holder GE,Vaegan. 2004. Visual evoked potentials standard (2004). Doc Ophthalmol 108:115–123.

Ortiz E, Pasquini JM, Thompson K, Felt B, Butkus G, Beard J, Connor JR. 2004. Effect of manipulation of iron storage, transport, or availability on myelin composition and brain iron content in three different animal models. J Neurosci Res 77:681–689.

Paez PM, Marta CB, Moreno MB, Soto EF, Pasquini JM. 2002. Apotransferrin decreases migration and enhances differentiation of oligodendroglial progenitor cells in an in vitro system. Dev Neurosci 24:47–58.

Taylor EM, Morgan EH, 1990. Developmental changes in transferrin and iron uptake by the brain in the rat. Brain Res Dev Brain Res 55:35–42.

Todorich B, Zhang X, Slagle-Webb B, Seaman WE, Connor JR. 2008. Tim-2 is the receptor for H ferritin on oligodendrocytes. J Neurochem 107:1495–1505.

Yu GS, Steinkirchner TM, Rao GA, Larkin EC. 1986. Effect of prenatal iron deficiency on myelination in rat pups. Am J Pathol 125:620–624.